Kinetic studies on the CO oxidation on a Rh(111) surface by means of angle-resolved thermal desorption

Tatsuo Matsushima, Toshiji Matsui, and Masanori Hashimoto
Research Institute for Catalysis, Hokkaido University, Sapporo 060, Japan

(Received 13 January 1984; accepted 2 July 1984)

The kinetics of the reaction of adsorbed CO with oxygen adatoms was studied in the temperature range of 100–600 K with LEED and angle-resolved thermal desorption. At small oxygen coverages the CO_2 formation peaked from 500 to 400 K with increasing CO exposure. The activation energy decreased from 45 to 35 kcal/mol. When the oxygen coverage was large, a new CO_2 formation peak appeared around 400 K. The activation energy was 30 kcal/mol. LEED observations revealed that the surface was covered by separate domains of CO and oxygen. The former CO_2 is produced outside the domains or on the perimeters, whereas the latter is formed in the oxygen domains. The angular distribution of the desorption of CO_2 in the former varied as $\cos^4\theta$, where θ is the desorption angle. The desorption of CO_2 in the latter showed a sharper angular distribution of $\cos^{15}\theta$.

I. INTRODUCTION

The energy distribution of desorbing product molecules gives a microscopic insight into the dynamics of surface reactions. The determination of the angular distribution of the desorption flux is the first step in the analysis of the translational energy.[1,2] From this distribution, it can be examined whether the product is trapped on the surface after the formation. If it is trapped, the molecule would lose kinetic information of the reaction. On the other hand, it would hold information in the energy states, if it desorbs directly from the activated state. In this case the angular distribution at times becomes sharp along the surface normal, i.e., desorbing molecules have an excess translational energy perpendicular to the surface. Recent work by Comsa's group[3–6] has shown that a simple one-dimensional model proposed by Willigen[1] can be used as a prototype to explain the angular and velocity distributions. This model, however, must be modified by considering several factors, i.e., the vibrational modes of activated complexes,[7] the interaction between gas molecules and surfaces,[8,9] and the potential energy profiles in the neighborhood of desorption sites.[10] The potential energy converted into the translational form can be roughly estimated from the angular distribution.[3,5]

The CO oxidation over noble metals is a suitable model for this kind of study, because the product CO_2 interacts only weakly with the surfaces.[11–15] On Pt, the angular distribution is very sharp along the surface normal,[16,17] whereas it follows a simple cosine form on Pd.[18] Time of flight measurements[19] with a Pt foil at 880 K revealed that the product CO_2 desorbed perpendicular to the surface held an excess translational energy of about 7 kcal/mol. The above results were obtained by molecular beam scattering. This method can be applied only at relatively high temperatures, where the steady product formation is significant. On the other hand, the angle-resolved thermal desorption[12,14] is useful for a study over a wide coverage range of the reactants and at low temperatures. In a previous paper[14] we reported the angular distribution of the desorption of CO_2 produced on polycrystalline rhodium surfaces. CO_2 produced by heating coadsorbed layers of CO and oxygen showed two peaks, depending on the surface coverages. The desorption of CO_2 in the two peaks showed very sharp and different angular distributions. Neither kinetic analysis of the reaction rate, nor precise determination of the angular distribution was given, because these peaks overlapped. In the present paper, we will report a detailed analysis of the kinetic results on a Rh(111) surface and the angular distribution of CO_2 desorption, where the two CO_2 peaks can be separately studied. Furthermore, the adsorption structures are analyzed.

II. EXPERIMENTAL

The experimental apparatus and procedures were essentially the same as those reported previously.[12,14] Briefly, the apparatus consisted of a reaction chamber, an analyzer chamber, and a collimator placed between them. These were all separately pumped out. The first had LEED-AES optics, an Ar^+ gun and a mass spectrometer. The single crystal sample was a disk-shaped slice (7 mm diameter$\times$0.5 mm thickness, purity 99.995% from Metal Crystal Ltd., UK). Both faces were polished with standard metallographic techniques. The sample was set on a rotatable axis perpendicular to the axis of the collimator.

The sample covered by O_2 and/or CO was resistively heated, while the amount of O_2, CO, or CO_2 passing through the collimator was monitored with a mass spectrometer in the analyzer chamber (angle-resolved spectra). Desorption spectra were also recorded in an angle-integrated form with a mass spectrometer in the reaction chamber. The latter was used to analyze general features of the CO_2 formation and the kinetics of the reaction. The other was used for the determination of the angular distribution of the CO_2 desorption. The signal in the angle-integrated form involves the contribution from the side of the sample ($\sim$12% of the total area.)

III. RESULTS

A general overview of the CO_2 formation will be summarized in the first section. The other sections will deal in detail with the kinetics of CO_2 formation, angular distribution of the CO_2 desorption, and adsorption structure analysis by LEED.

 0021-9606/84/235151-10$02.10

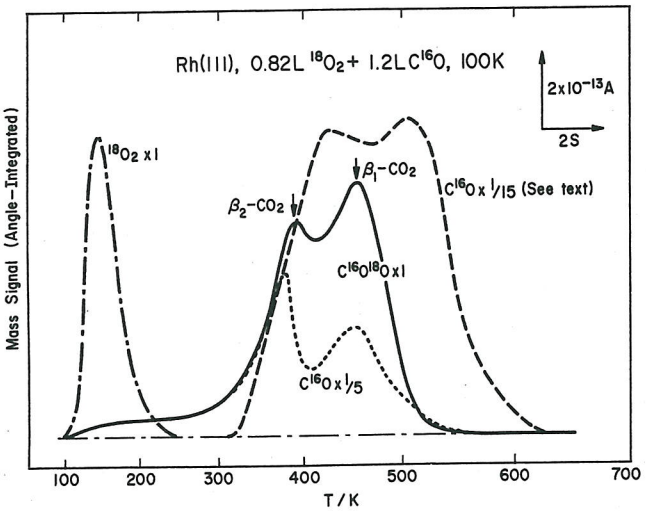

FIG. 1. Typical thermal desorption spectra of $^{18}O_2$, C ^{16}O, and C ^{16}O ^{18}O when the surface was exposed to 0.82 L $^{18}O_2$ and 1.2 L C ^{16}O at 100 K. The dashed curve of CO shows the desorption from a CO-saturated surface without O_2 exposure. The heating rate was 33 K/s.

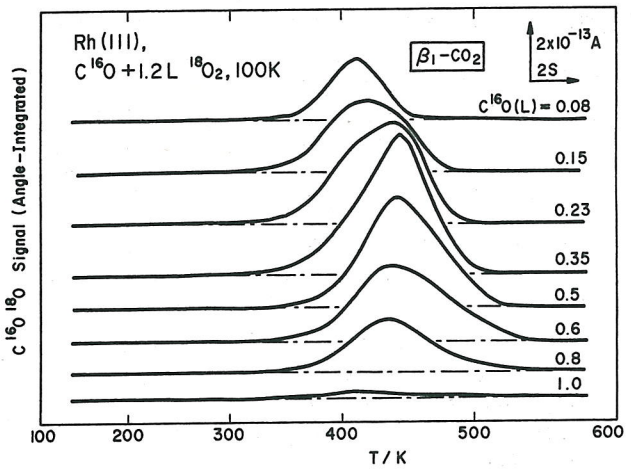

FIG. 2. Variation of CO_2 spectra with various CO preexposures. The surface was first exposed to CO and then to 1.2 C $^{18}O_2$ at 100 K. The heating rate was 20 K/s.

A. General features

The general features of CO_2 formation on polycrystalline Rh surfaces[14] were reproduced on the well-defined (111) surface. The CO_2 formation spectra depended strongly on the amount of CO and O_2 exposure, adsorption temperature, and exposure sequence. Typical spectra (in the angle-integrated form) of the desorption of CO, O_2, and CO_2 are shown in Fig. 1. The surface was exposed to 0.82 L (Langmuir) $^{18}O_2$ (the coverage relative to the saturation value determined by TDS was 0.60) at 100 K and further to 1.2 L C ^{16}O (frequently oxygen 16 is simply designated as O). It was heated at a constant current up to 1400 K. The temperature increased linearly with a rate of 33 K/s below 700 K. The exposure pressure was 2.4×10^{-8} Torr for $^{18}O_2$ and 1.0×10^{-8} Torr for CO. C ^{16}O ^{18}O was produced in the temperature range of 300–500 K. This range is very narrow as compared with that on polycrystalline surfaces.[14] Neither C $^{16}O_2$ nor C $^{18}O_2$ was observed. The usage of $^{18}O_2$ improved the ratio of the signal to the noise of the mass spectrometer highly in the analyzer chamber, because the noise in the CO_2 signal was caused by fluctuation of the background level of C $^{16}O_2$. C ^{16}O ^{18}O peaked around 460 K (β_1-CO_2) and 390 K (β_2-CO_2). The reaction product C ^{16}O ^{18}O is frequently designated as CO_2 in the text. The predominance of β_1- or β_2-CO_2 depended on O_2 and CO exposure. No α-CO_2 formation from the interaction between oxygen admolecules and CO[12] was observed. This is probably due to the small amount of molecular oxygen on Rh(111).[20,21] The O_2 desorption peaked around 160 K. Another O_2 desorption was observed above 800 K when CO exposure was small. The former has been assigned to the desorption from adsorbed molecular oxygen.[20,21] The other is due to the desorption from oxygen adatoms.[20–22] CO showed two desorption peaks around 380 and 450 K. The former appeared only when O_2 and CO exposure was large. The latter was attenuated rapidly with increasing exposure of oxygen. By way of comparison, a spectrum of CO which was desorbed from CO saturated surface without oxygen exposure (2.4 L CO at 100 K) is shown in the figure. It should be noticed that the pumping rate for CO_2 in the reaction chamber was about twenty times as large as that of CO.

When CO was first dosed, the CO_2 spectrum showed a simple behavior. Typical results are summarized in Fig. 2. The amount of CO_2 produced increased first with CO exposure and showed its maximum around 0.35 L CO. After this point, it decreased and disappeared above 1.0 L. In this case

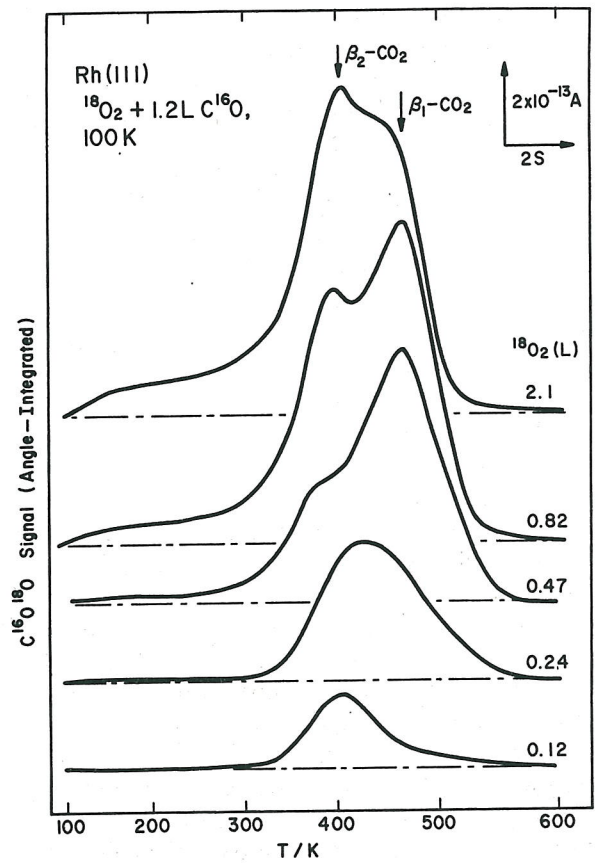

FIG. 3. CO_2 formation spectra with various amounts of $^{18}O_2$ exposures followed by 1.2 L exposure of C ^{16}O at 100 K. The heating rate was 35 K/s.

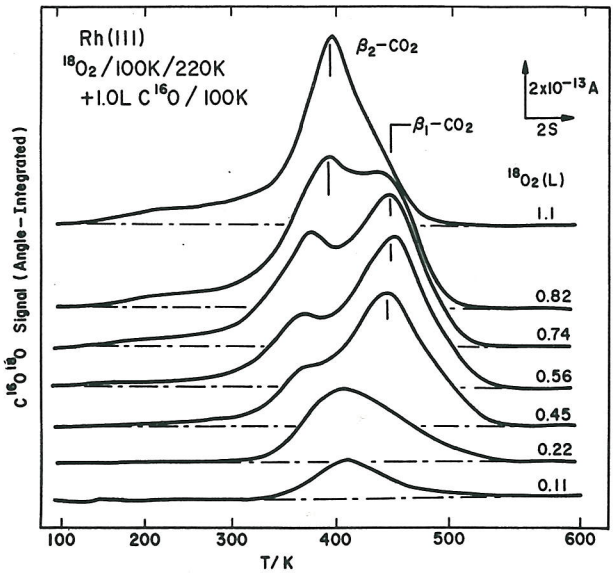

FIG. 4. CO_2 formation spectra with various amounts of $^{18}O_2$ exposure at 100 K followed by heating up to 220 K, and 1.0 L exposure of C ^{16}O at 100 K. There is an improved separation of β_1-CO_2 from β_2-CO_2. The heating rate was 28 K/s.

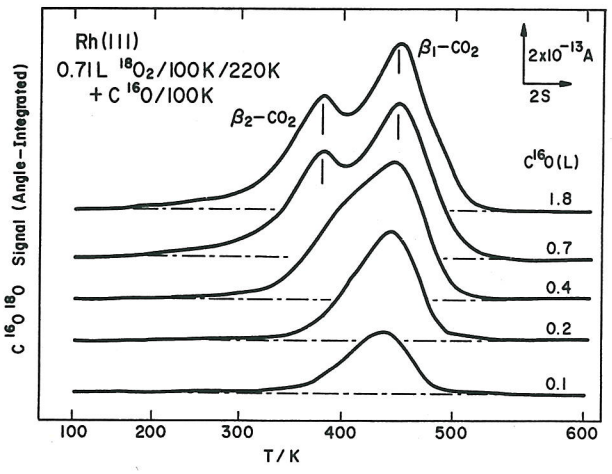

FIG. 6. β_1-CO_2 and β_2-CO_2 formation spectra at moderate O_2 exposures. The heating rate was 23 K/s.

only β_1-CO_2 was produced. The separation of β_2-CO_2 from β_1-CO_2 became clearer when the surface temperature was raised once up to 220 K after O_2 exposure at 100 K. CO_2 spectra with various O_2 exposures without such preheating are summarized in Fig. 3. The surface was exposed to various amounts of oxygen and 1.2 L CO at 100 K. A single peak (β_1) was observed around 400 K at small O_2 exposures. Above 0.47 L O_2 the spectrum became broad with an increase in O_2 exposure and showed a shoulder of β_2-CO_2 around 400 K. The peak temperature of β_1-CO_2 shifted from 400 to 470 K. When the surface exposed to O_2 in large amounts (>2.0 L O_2), β_2-CO_2 became predominant, but β_1-CO_2 was still significant. On the other hand, β_1-CO_2 mostly disappeared when the surface was heated once to 220 K after large O_2 exposure. Typical CO_2 spectra are shown in Fig. 4. In this case the surface was exposed to various amounts of oxygen at 100 K and heated up to 220 K. 1.0 L CO was introduced after cooling down to 100 K. No changes in general features were observed. The β_1-CO_2 peak shifted from 400 to 450 K with increasing CO exposure. Only β_2-CO_2 was observed above 1.1 L preexposure of oxygen, where the surface was saturated with oxygen. The better β_1–β_2 separation was quite reproducible. From now on, the surface was heated up to 220 K after O_2 exposure except for experiments of LEED. β-CO_2 is formed through the interaction between adsorbed CO and oxygen adatoms, since oxygen is dissociatively adsorbed above 200 K.[20–22]

Kinetic analysis was carried out in following three regions: (i) Small O_2 exposures. The spectra below 0.35 L preexposure of oxygen showed a single β_1-CO_2 peak, as shown in Fig. 5. The peak temperature shifted from 480 to 430 K with increasing CO exposure.

(ii) Moderate O_2 exposures. CO_2 spectra observed at 0.7 L preexposure of oxygen and various CO exposures are shown in Fig. 6. When CO exposure was small, only the β_1-

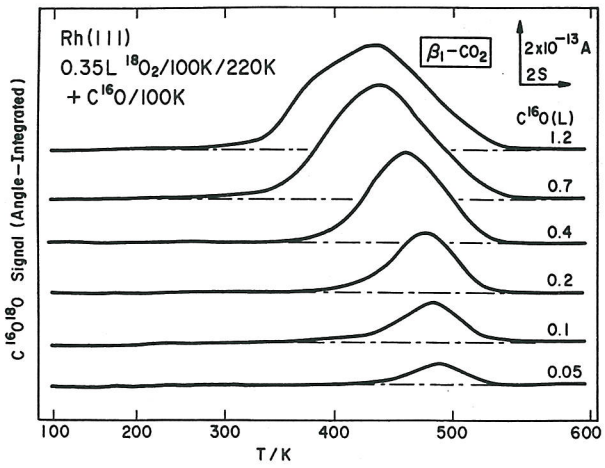

FIG. 5. β_1-CO_2 formation spectra at small O_2 exposures. The surface was exposed to 0.35 L $^{18}O_2$ at 100 K and heated to 220 K. It was further exposed to various amounts of CO at 100 K. The heating rate was 22 K/s.

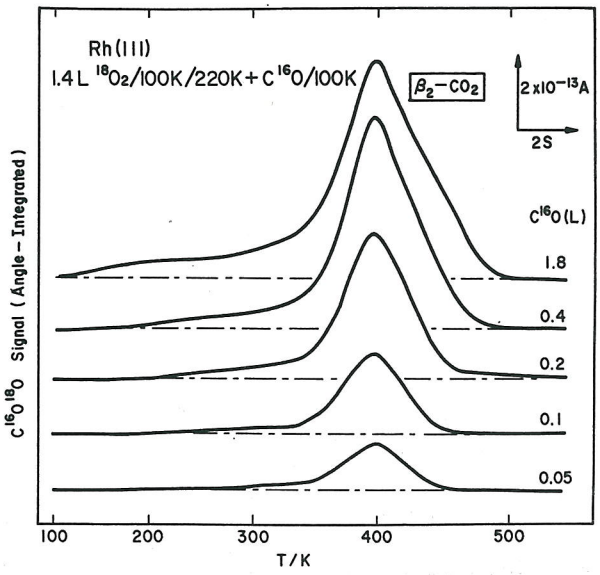

FIG. 7. β_2-CO_2 formation spectra on oxygen-saturated surfaces. The heating rate was 24 K/s.

CO_2 peak appeared. A shoulder of β_2-CO_2 grew with CO exposure. β_1-CO_2 remained predominant at large CO exposures.

(iii) Large O_2 exposures. CO_2 formation spectra on oxygen-saturated surfaces are shown in Fig. 7. Only β_2-CO_2 was produced irrespective of CO exposures. No shift of the peak temperature was observed.

B. The activation energy

The activation energy of CO_2 formation was estimated by using an isostere method.[23] Analysis by means of Redhead's equations[24] was not performed because the reaction orders with respect to CO and oxygen were not considered to be constant over a wide range of coverages. In the isostere method, the activation energy is determined from the slope of the logarithm of the desorption rate (reaction rate) measured in a large pumping system against the reciprocal of the temperature at fixed coverages. In the present analysis the logarithm of the peak maximum (the maximum CO_2 formation rate) was plotted against the reciprocal of the peak temperature because the amount of CO_2 produced was independent of the heating rate and the CO_2 peak was fairly symmetrical. The activation energy was determined at three different oxygen exposures. The heating rate ranged from 4 to 150 K/s. Representative sets of reaction isosteres for the CO_2 formation rate are shown in Figs. 8–10. When the oxygen exposure was small, the activation energy for β_1-CO_2 formation ranged from 45 to 35 kcal/mol with increasing CO exposure, as shown in Fig. 8. At moderate O_2 exposures, the activation energy of β_1-CO_2 remained almost constant around 45 kcal/mol independent of CO exposure (Fig. 9). Figure 10 shows that the activation energy of β_2-CO_2 forma-

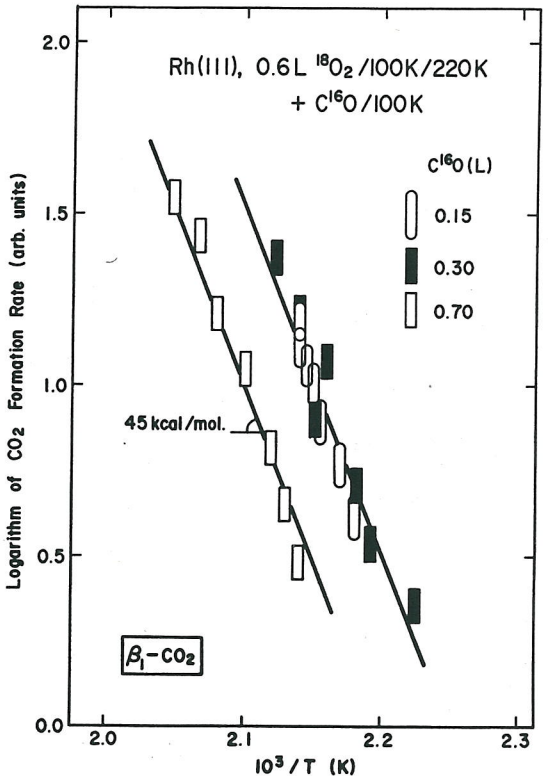

FIG. 9. β_1-CO_2 reaction isosteres at moderate O_2 exposures.

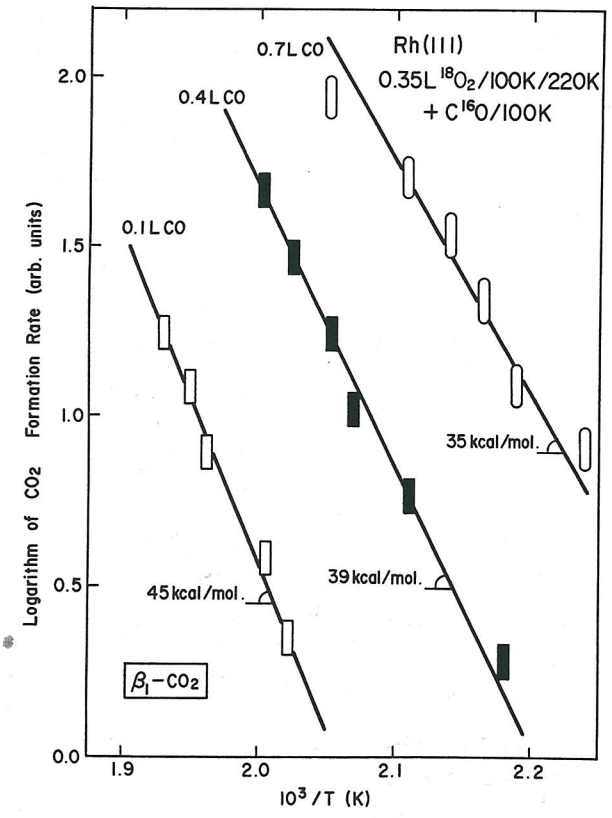

FIG. 8. CO_2 reaction isosteres at small O_2 exposures. The slope of the linear isostere indicates the activation energies ranging from 35 kcal/mol for 0.7 L CO to 45 kcal/mol for 0.1 L CO.

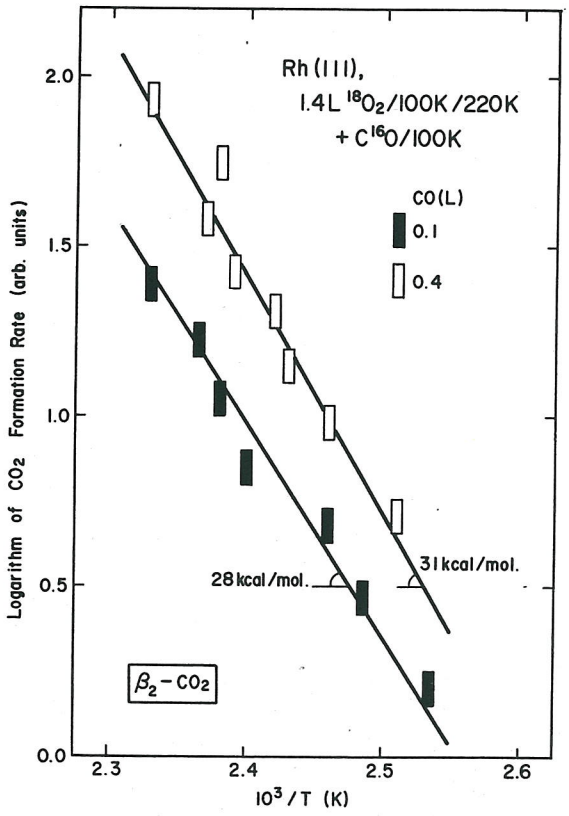

FIG. 10. β_2-CO_2 reaction isosteres on oxygen-saturated surfaces.

tion on oxygen-saturated surfaces was about 30 kcal/mol, independent of CO exposure.

C. Angular distribution of CO_2 desorption

Figure 11 shows CO_2 spectra observed at various desorption angles at moderate oxygen exposures. The upper panel shows the angle-resolved spectra and the bottom shows the angle-integrated form. The surface was exposed to 0.6 L $^{18}O_2$ at 100 K and heated up to 220 K. C ^{16}O of 1.2 L was introduced at 100 K and heated with a rate of 56 K/s. The CO_2 spectrum in the angle-integrated form shows predominantly β_1-CO_2 and a small contribution from β_2-CO_2. It shows the total amounts of β_1- and β_2-CO_2 formation. On the other hand the CO_2 spectrum in the angle-resolved form at $\theta = 0$ (θ is the desorption angle between the surface normal and the collimator axis) consisted of almost equal intensity of β_1-CO_2 and β_2-CO_2. This means that the desorption of β_2-CO_2 is distributed along the surface normal more sharply than β_1-CO_2. The peak height of β_2-CO_2 decreased with increasing θ more rapidly than that of β_1-CO_2. The angular distribution of β_1-CO_2 showed $\cos^4\theta$ dependence. The distribution from the other was sharper than $\cos^8\theta$. The determination was not reliable in this region, since the β_2-CO_2 peak was obscured by the large β_1-CO_2 peak at large desorption angles. The angular distribution of β_1-CO_2 was studied below 0.6 L O_2, since in this region the β_1-CO_2 formation

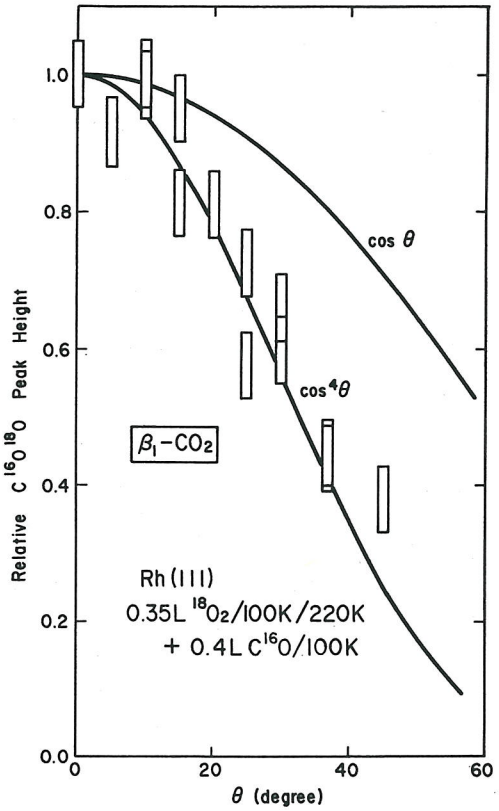

FIG. 12. Angular distribution of the β_1-CO_2 formation.

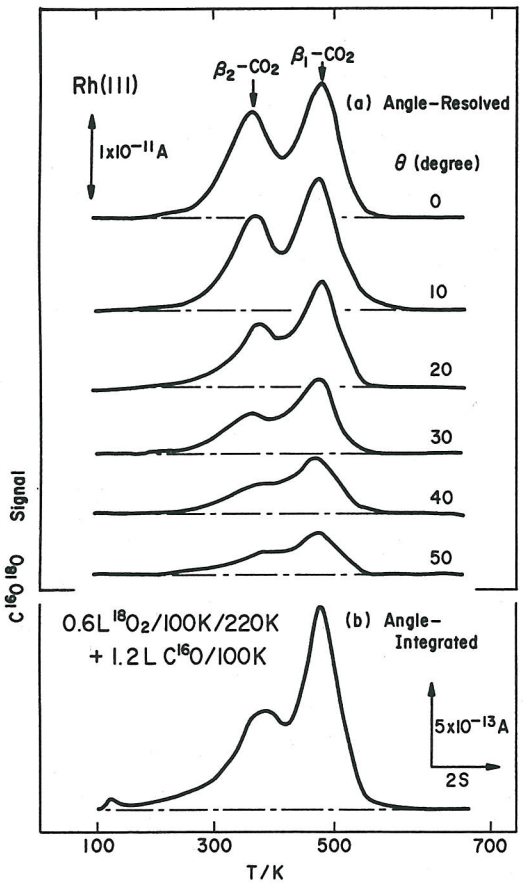

FIG. 11. (a) Angle-resolved CO_2 formation spectra observed at various desorption angles. (b) A CO_2 formation spectrum in the angle-integrated form observed simultaneously. The heating rate was 57 K/s.

was predominant. The results obtained at 0.35 L O_2 are summarized in Fig 12, where the relative CO_2 peak height is plotted against the desorption angle. The angular distribution varied as $(\cos\theta)^{4\pm1}$. The distribution did not vary within the range of 0.2–0.6 L preexposure of $^{18}O_2$ and 0.1–1.2 L postexposure of CO. This angular distribution agreed well with previous results on polycrystalline surfaces.[14] The angular distribution of β_2-CO_2 desorption was determined at 1.4 L preexposure of O_2. Typical CO_2 spectra are shown in Fig. 13. The surface was heated up to 220 K after 1.4 L preexposure of $^{18}O_2$ and exposed to 0.4 L C ^{16}O at 100 K. The heating rate was 90 K/s. The upper panel shows the

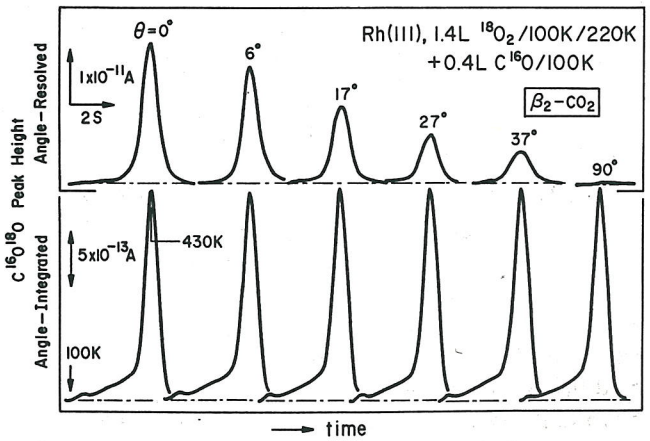

FIG. 13. Typical β_2-CO_2 formation spectra in the angle-resolved form (upper) and also in the angle-integrated form (lower) at various desorption angles. The heating rate was 90 K/s.

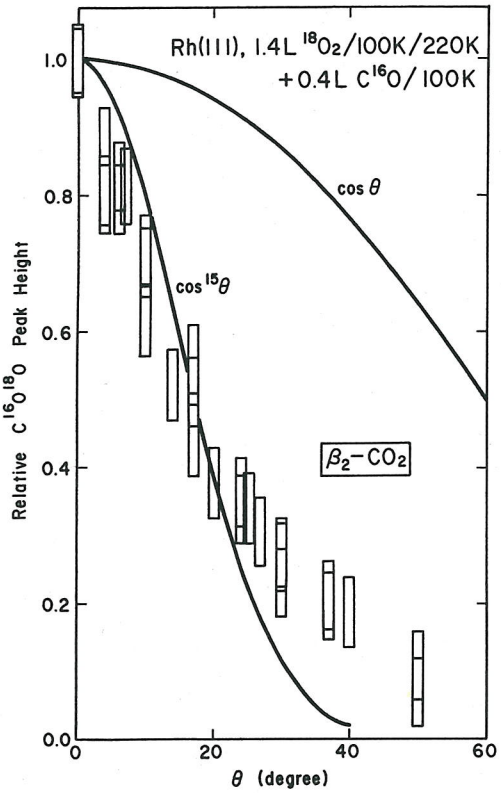

FIG. 14. Angular distribution of the β_2-CO_2 formation. The heating rate was 90 K/s.

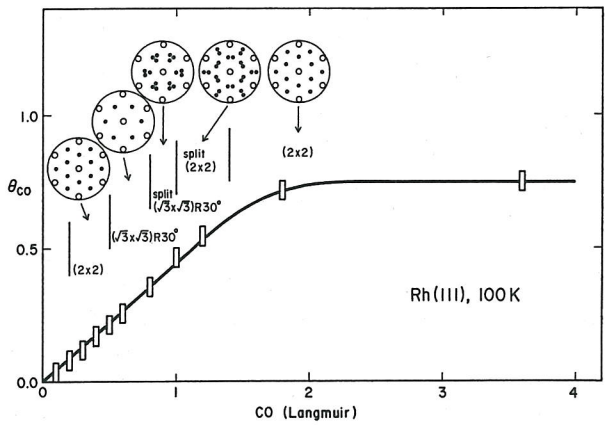

FIG. 15. CO coverage and LEED pattern vs exposure. Open and closed circles indicate diffraction spots due to the base metal and adsorbates, respectively.

angle-resolved CO_2 spectra recorded in the analyzer chamber. The peak height decreased very rapidly with an increase in the desorption angle. The lower panel summarizes the angle-integrated CO_2 spectra simultaneously recorded in the reaction chamber. These spectra remained invariant. The signal intensity can not be directly compared with that in the analyzer chamber, because the amplifier system of the two mass spectrometers were different. The relative value of the signal in the angle-resolved spectra is plotted against the desorption angle in Fig. 14. The vertical rectangles indicate the limit of experimental errors. The angular distribution was extremely sharp and varied as $(\cos\theta)^{15\pm3}$. This is much sharper than on polycrystalline surfaces.[14] Such sharper distributions on single crystal surfaces were observed on Pt.[12] This distribution did not depend on the heating rate in the range of 10–140 K/s. No coverage dependence was observed in the range of 0.1–1.2 L CO exposure.

D. LEED data

LEED patterns were always observed at 100 K. A faint (2×2) structure appeared after O_2 exposure at 100 K. The spot intensity increased remarkably after heating up to 220 K. This heating removed molecular oxygen[20,21] and led to a well-ordered (2×2)-O structure.[22] When a clean surface was exposed to CO at room temperature, a (√3×√3)R30° [abbreviated below to (√3)R30] structure first appeared[25] around 0.5 L and the intensity reached its maximum around 1.0 L. On the other hand, a (2×2) structure was observed at 0.2 L CO at 100 K.[26] This structure coexisted with the (√3)R30 around 0.45 L. Above this exposure the (√3)R30 spot was very sharp. Above 0.8 L CO, the spot became broad and split. Finally another (2×2) structure appeared above 1.4 L CO after split (2×2). The (2×2) structure appearing at 0.2 L CO has a one-fourth monolayer of CO (the CO coverage $\theta_{co} = 1/4$) and the final (2×2) a three-fourth monolayer ($\theta_{co} = 3/4$).[26] Figure 15 summarizes these results. Vertical bars indicate transition regions around which neighboring patterns were observed simultaneously. The transition from split (√3)R30 to split (2×2) was associated with other complex patterns. The amount of CO(a) was determined by thermal desorption. The maximum amount was adjusted to the coverage = 3/4.[26] The reverse sequence of the LEED patterns was well reproduced when the surface saturated with CO was heated sequentially to reduce the amount of CO(a).

LEED patterns showed a complicated behavior when the surface was exposed to both reactants. The superposition of the (2×2)-O and (√3)R30-CO was observable when the surface coverages were suitably controlled. The results are listed in Tables I and II. In the former series of experiments the surface was first exposed to CO and further to 1.4 L O_2 at 100 K. It was heated to desired temperatures and again cooled down to observe LEED patterns. The temperature was raised to the region in which CO_2 was formed. In general, CO adsorption structures were converted to those at higher CO coverages by O_2 adsorption. At 0.4 L CO, (2×2)-CO was converted to the superposition with (√3)R30-CO after O_2 adsorption. At 0.5 L the sharp (2×2)-CO disappeared. At 0.6–0.7 L CO, the sharp (√3)R30-CO was split. These results suggest that CO domains are compressed by O_2 adsorption. After annealing to 390 K, sharp (2×2)-O appeared when adsorbed oxygen was significant. For example at 0.6 L CO, split (√3)R30-CO was replaced by the superposition of sharp (2×2) and (√3)R30-CO. After heating to 440 K, the (2×2) and (√3)R30-CO were observed at almost the same intensity. Further heating lowered the intensity of (2×2) below that of (√3)R30-CO and then (2×2) > (√3)R30-CO. The former (2×2) below 440 K can be assigned to (2×2)-O and the latter (2×2) (above 486 K) to (2×2)-CO at $\theta_{co} = 1/4$, because (√3)R30-CO never coexists with (2×2)-CO at $\theta_{co} = 3/4$, and further (2×2)-CO at $\theta_{co} = 1/4$ follows (√3)R30-CO when CO coverage decreases. The LEED pat-

TABLE I. LEED patterns when the surface was exposed to various amounts of CO and then to 1.4 L O_2 at 100 K. The surface was sequentially heated to 500 K. LEED patterns were observed at 100 K. The maximum intensity of the spots was compared in the range of 20–60 eV of the beam energy.[a]

	+ 1.4 L O_2	Annealing temperature (K)					
CO(L)	100	100	390	440	465	486	500
0.4	s(2)	(2) + b($\sqrt{3}$)	s(2)	s(2)	s(2)	b(2)	clean
($\theta_{co} = 0.20$)							
0.5	s(2) > s($\sqrt{3}$)	b($\sqrt{3}$)	s(2) + f($\sqrt{3}$)	s(2) + f($\sqrt{3}$)	b(2) + f($\sqrt{3}$)	f(2)	clean
($\theta_{co} = 0.25$)							
0.6	s($\sqrt{3}$)	sp($\sqrt{3}$)	s(2) ≫($\sqrt{3}$)	(2) + ($\sqrt{3}$)	(2) < ($\sqrt{3}$)	(2) > ($\sqrt{3}$)	f(2)
($\theta_{co} = 0.30$)							
0.7	s($\sqrt{3}$)	sp($\sqrt{3}$)	sp($\sqrt{3}$)	b($\sqrt{3}$)	s($\sqrt{3}$)	s(2) ≫($\sqrt{3}$)	f(2)
($\theta_{co} = 0.35$)							
0.9	(no O_2 exposure) sp($\sqrt{3}$)		sp($\sqrt{3}$)	sp($\sqrt{3}$)	s($\sqrt{3}$)	s(2) > ($\sqrt{3}$)	f(2)
($\theta_{co} = 0.45$)							

[a] θ_{co}; CO coverage. LEED pattern; (2) = (2×2), ($\sqrt{3}$) = ($\sqrt{3}\times\sqrt{3}$)R 30°. Diffraction spot; +: coexistence, <: more intense, ≪: much more intense, s: sharp, b: broad, f: faint, and sp: split.

tern sequence with a decreasing amount of CO(a) is listed at the bottom of the table, where the surface was exposed to only 0.9 L CO and heated sequentially. The above results can be explained by assuming that the surface is essentially covered by separate domains of CO and oxygen adatoms, as follows:

(i) CO(a) < O(a), i.e., 0.4 L CO. (2×2)-O domains remain throughout heating procedures. The superposition of (2×2)-O and ($\sqrt{3}$)R30-CO is not confirmed.

(ii) CO(a) ≳ O(a), i.e., 0.5–0.6 L CO. ($\sqrt{3}$)R30-CO domains are predominant at low temperatures. Heating to 390 K results in a well-ordered (2×2)-O. By annealing to 440–465 K, O(a) domains are consumed and ($\sqrt{3}$)R30-CO becomes sharp. Further heating reduces the CO coverage, yielding (2×2)-CO at $\theta_{co} = 1/4$.

(iii) CO(a) ≫ O(a), i.e., above 0.7 L CO. The surface shows LEED patterns almost the same as those without O_2 exposures.

Table II lists LEED patterns when CO was exposed after O_2 exposure at 100 K and annealing to 220 K. Above 0.7 L O_2, only the (2×2)-O structure was observed even after CO exposure. The intensity was increased by annealing above 300 K. No ($\sqrt{3}$)R30-CO was observed. The superposition of the two structures was observed at 0.35 L O_2 or less. The (2×2)-O became broad after CO exposure at 100 K. When CO exposure was 0.9 L, the superposition of sharp (2×2) and ($\sqrt{3}$)R30-CO was observed, after annealing to 390 K. The intensity of the (2×2) first decreased and that of ($\sqrt{3}$)R30-CO increased. Furthermore, the (2×2) became intense more than ($\sqrt{3}$)R30-CO. For the same reason described

TABLE II. LEED patterns observed when O_2 and then CO were dosed. The surface was first exposed to various amounts of O_2 and annealed to 220 K. It was further exposed to CO at 100 K and heated sequentially. LEED patterns were observed at 100 K.[a]

		Annealing temperature (K)					
O_2(L)	+ CO(L)	100	390	440	465	485	500
0.35	0.3	b(2)	s(2)	s(2)	b(2)	f(2)	clean
($\theta_0 = 0.25$)							
	0.9	(2)	(2) + ($\sqrt{3}$)	(2) < ($\sqrt{3}$)	(2) > ($\sqrt{3}$)	f(2)	clean
	1.2	b(2)	sp($\sqrt{3}$)	s(2) + ($\sqrt{3}$)	b(2) < ($\sqrt{3}$)	(2) > ($\sqrt{3}$)	f(2)
0.71	1.2	(2)	(2)	(2)	(2)	(2)	(2)
($\theta_0 = 0.50$)							
1.4	1.2	(2)	(2)	(2)	(2)	(2)	(2)
($\theta_0 = 0.87$)							

[a] θ_0: oxygen coverage relative to the maximum thermal desorption peak area. The other notations; see Table I.

above, the (2×2) below 440 K can be assigned to (2×2)-O and the (2×2) above 465 K to (2×2)-CO at $\theta_{co} = 1/4$. The results can be explained as follows: When CO(*a*) < O(*a*), i.e., 0.35 L O_2 and 0.3 L CO, or above 0.7 L O_2, (2×2)-O domains are predominant throughout the above procedures. At CO(*a*) > O(*a*), i.e., 0.35 L O_2 and 0.9–1.2 L CO, (2×2)-O and ($\sqrt{3}$)R30-CO domains coexist. Further heating removes oxygen adatoms, producing ($\sqrt{3}$)R30-CO and then (2×2)-CO at $\theta_{co} = 1/4$. It can be concluded that the surface is essentially covered by separate domains of CO(*a*) and O(*a*).

IV. DISCUSSION

In this section we will discuss the mechanism of the formation of β_1-CO_2 and β_2-CO_2, and also their angular distributions.

A. Reaction mechanism

The present experimental results of CO_2 formation are essentially the same as those on polycrystalline Rh.[14] On polycrystalline Rh, however, CO_2 formation started at temperatures much lower than on Rh(111). Significant CO_2 formation from coadsorbed layers of CO(a) and O(a) was noticed in the range of 150–500 K on polycrystalline Rh. The peak positions of β_1–CO_2 and β_2-CO_2 were around 300–400 and 300 K, respectively. On Rh(111), β_1- and β_2-CO_2 peaked in the range of 400–500 and around 400 K. Similar phenomena have been reported on platinum. On Pt(111)[12,27] CO_2 formation peaked around 300 K with a narrow peak width. On the other hand CO_2 showed broad peaks in the range of 100–400 K on stepped (321) surfaces.[28] Such broad CO_2 peaks were rationalized by proposing that the activation energy for reaction of terrace and step CO with terrace and step atomic oxygen was sufficiently different.[28] Therefore it is likely that the activation energy determined on polycrystalline Rh[29–31] is smaller than that on Rh(111).

Two CO_2 formation peaks are reminiscent of similar phenomena on Pd(111) at low temperatures reported by Conrad *et al.*[32] They observed surface processes for CO_2 formation quite similar to the β_1-CO_2 and β_2-CO_2 in the present work. They concluded from LEED, UPS, and TDS experiments that under certain conditions the CO admolecules and oxygen adatoms form separate domains and a true coadsorbate phase, depending on the amount of CO exposure. The former (separate domains) yielded a CO_2 desorption peak at temperatures higher than that from the latter (coadsorbate phase). The reaction mechanism on Rh(111) is essentially the same as in this model. Over Rh(111), oxygen adatoms coalesce into domains of the (2×2) structure. This island formation is accelerated by heating the surface above 200 K.[22] After this heating the surface is partially covered by oxygen domains of the (2×2) structure. CO is adsorbed preferentially on the clean parts outside the domains. The surface is covered by separate domains of CO and oxygen. The interaction between CO(*a*) and O(*a*) occurs outside the domains or on the perimeters. This interaction yields β_1-CO_2. When the oxygen coverage is small, the oxygen domains are also small and distributed randomly. The kinetics of β_1-CO_2 formation behaves like a second order reaction, i.e., the peak position of

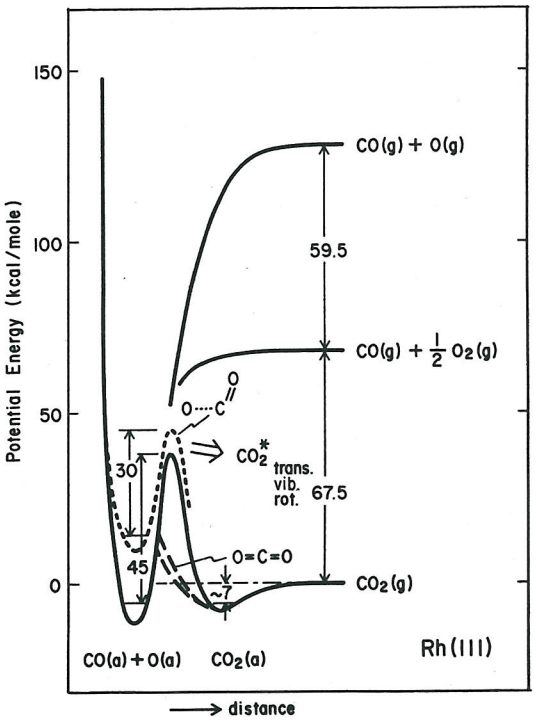

FIG. 16. Potential energy diagram for CO_2 formation. All energies are in kcal/mol.

CO_2 shifts to lower temperatures with increasing CO exposure (Fig. 5). When the oxygen coverage increases, the oxygen domains grow. The interaction between CO(*a*) and O(*a*) occurs mostly on the perimeters of oxygen domains. The surface diffusion of the reactants is limited by large domains of oxygen. Therefore the kinetics is no longer akin to a second order reaction. When CO exposure is increased, CO begins adsorbing in oxygen domains. These CO admolecules interact strongly with oxygen adatoms, since the distance of CO(*a*) to O(*a*) is short. This interaction is probably repulsive.[32] Hence the adsorption energy of CO(*a*) and O(*a*) will be reduced. The activation energy of CO_2 formation is reduced and the resultant β_2-CO_2 is formed at lower temperatures. When the surface is initially saturated with oxygen adatoms, CO is not adsorbed on clean surfaces. CO is adsorbed in the oxygen domains, so that only β_2-CO_2 is formed even at small CO exposures. When CO is first dosed, only β_1-CO_2 is formed. In this case CO cannot adsorb in oxygen domains.

A potential energy diagram illustrating the CO_2 formation is shown in Fig. 16. The abscissa (distance from the surface) is drawn only in a qualitative sense. The initial state of the CO_2 formation consists of CO(*a*) and O(*a*). The potential energy of this state can be evaluated from the heat of adsorption of CO and O_2. Thiel *et al.* found that the initial heat of adsorption of CO on Rh(111) is 31.6 kcal/mol.[26] The initial heat of dissociative adsorption of oxygen is 85 kcal/mol on Rh(100).[20] The heat of the adsorption on Rh(111) by Thiel *et al.*, 56 kcal/mol,[22] was not used here, since the initial dissolution of oxygen was noted to be significant. The energy of CO(*a*) + O(*a*) is 74.1 kcal/mol below the level of CO(*g*) + 1/2 O_2(*g*). The heat of the reaction CO(*g*) + 1/2 O_2(*g*)→CO_2(*g*) is 67.5 kcal/mol.[33] The dissociation energy of

O_2 is 119 kcal/mol.[33] The energy level of $CO_2(g)$ is adjusted to zero.

The activation energy of β_1-CO_2 formation at small exposures was 45 kcal/mol. It decreased to 35 kcal/mol at large CO exposures. This decrease may be attributed to the increased repulsion between coadsorbed reactants.[17,18] The potential energy of the activated complex is much higher than the heat of adsorption of CO_2, 6–7 kcal/mol.[14] Therefore desorbed CO_2 may have higher internal or kinetic energies than when it is in equilibrium with the surface temperature. β_2-CO_2 is formed from the interaction between O(a) and CO(a) in the oxygen domain. The energy shift of the initial state was estimated as 20 kcal/mol. The heat of adsorption of CO in the oxygen domains was estimated to be 23 kcal/mol from the low temperature peak of CO in Fig. 1. The heat of dissociative adsorption of oxygen is 60 kcal/mol at high oxygen coverages on Rh(100).[20] The activation energy for the β_2-CO_2 formation is 30 kcal/mol. This upward shift of the potential energy curve (drawn by the dotted line) yields an increase in the potential energy of the activated state by about 7 kcal/mol. This increment can produce a sharper angular distribution of CO_2 formation. The level of the zero point energy is drawn only for the adsorption states.

B. Angular distribution

The CO_2 desorption from the physisorption state shows a simple cosine distribution.[14] The sharp angular distribution of the reaction product indicates that it leaves the surface with an excess translational energy perpendicular to the surface, without being trapped in the physisorption state. The origin of such an excess translational energy of desorbing molecules was typically explained by a simple one-dimensional model proposed by Willigen.[1] The angular distribution is related to the activation barrier perpendicular to the surface. Recent work by Comsa's group[3–6] showed that this simple model still can be used as a prototype to explain the general features of the angular and velocity distributions. This model predicts that the mean kinetic energy of desorbing molecules increases with the increase in the desorption angle. Experiments, however, have shown the opposite trend.[19] Recently, Toya and his co-workers have succeeded in explaining the angular and velocity distribution of desorbing hydrogen molecules.[7] They used Willigen's model and introduced restricted vibrations of the activated complex parallel to the surface plane. The depth of this potential for restricted vibrations and also the potential energy of the activated complex can be determined from the detailed determination of the velocity distributions. Such experiments are not available at present, hence the Willigen model was used to roughly estimate the energy converted into the translational form. The desorption rate at each angle is a function of the ratio ϵ of the activation energy converted into the translational form E to the thermal energy at the surface temperature RT as follows:

$$I(\theta) = I(\theta = 0)\frac{\epsilon + \cos^2\theta}{(\epsilon + 1)\cos\theta} e^{-\epsilon \tan^2\theta},$$

$$\epsilon \equiv E/RT,$$

where $I(\theta)$ and $I(\theta = 0)$ are the desorption flux at θ and $\theta = 0$, respectively. From the angular distribution, ϵ was estimated to be 2 for the curve of $\cos^4\theta$. The peak temperature of β_1-CO_2 was 430–500 K. E is roughly 2 kcal/mol. The value for β_2-CO_2 is 6 kcal/mol. These values must be underestimated, since no restricted vibrations are considered.[7] They, however, may not be far from the true values. This energy essentially originates from the repulsive force between the surface and nascent CO_2 molecules. Stable linear CO_2 molecules are adsorbed in the physisorption state. The adsorption energy, 6–7 kcal/mol, is quite close to the heat of sublimation of solid carbon dioxide 8.4 kcal/mol. van der Waals' force plays a major role in the adsorption bonding. The equilibrium position is a few angstroms from the surface plane (van der Waals' radii). The position of the CO_2 formation is between the surface plane and the equilibrium position of the physisorption. The reactants CO(a) and O(a) are chemisorbed and their equilibrium positions are close to the surface. Nascent CO_2 molecules receive significant repulsive force the very instant that they are produced. This force increases the velocity of the product CO_2 along the surface normal. A potential energy curve yielding the above repulsive force is drawn by the dashed curves (designated by linear CO_2) in Fig. 16. The energy at the CO_2 formation position must be several kcal/mol above the $CO_2(g)$ level. When the coverages are increased, this potential energy curve will be shifted upward, because the distance from the position of the CO_2 formation to the adsorbates is shorter than to the surface metal. This can explain that the desorption of β_2-CO_2 produced in the oxygen domain is sharper than that of β_1-CO_2. The latter is produced outside the domain or on the perimeter. Therefore it is possible that the β_1-CO_2 formation occurs in an invariant chemical environment. The potential energy of the activated complex is about 38 kcal/mol for β_1-CO_2 and 45 kcal/mol for β_2-CO_2, relative to the $CO_2(g)$ level. The energy converted into the translational form is only several kcal/mol. The remnant energy is probably released in the vibrational and rotational form of nascent CO_2 molecules and also consumed by the interactions with surfaces. The latter involves rearrangements of surface atoms due to removal of oxygen adatoms and chemisorbed CO and also excitations of surface phonons. A bent configuration of the activated complex has been proposed by analysis of the kinetic isotope effect on the CO_2 formation rate over NiO.[34] Recent theoretical work predicted a similar configuration on Pt(111).[35] In this case the activation energy is partially used to change the angle of O(a) ···C = O(a), as well as to overcome the repulsion between O(a) and CO(a). Such an energy may be released in the internal form of CO_2. Recent experiments using infrared emission[36,37] revealed that the product molecules on polycrystalline Pt surfaces were vibrationally and also rotationally hotter than the surface. Their temperatures with a Pt foil at 775 K were estimated to be around 2000 K.[36] The excess internal energy is around 10 kcal/mol or less in this case. A similar situation may be predicted on Rh(111), since the adsorption behavior of CO and oxygen is quite similar to that on Pt(111). Furthermore the CO oxidation shows similar kinetics on both surfaces. Therefore it can be surmised that the

energy of the activated complex is mostly spent on the interactions with surfaces.

[1]W. van Willigen, Phys. Lett. A **28**, 80 (1968).
[2]G. Comsa, *Proceedings of the 7th International Vacuum Congress and 3rd International Conference Solid Surfaces*, edited by R. Dobrozemsky *et al.* (Vienna, 1977), p. 1317.
[3]G. Comsa and R. David, Chem. Phys. Lett. **49**, 512 (1977).
[4]G. Comsa, R. David, and B. J. Schumacher, *Proceedings of the 4 International Conference on Solid Surfaces and 3rd European Conference on Surface Sciences*, edited by D. A. Degras and M. Costa (Cannes 1980), p 252.
[5]G. Comsa, R. David, and B. J. Schumacher, Surf. Sci. **95**, L210 (1980).
[6]G. Comsa and R. David, Surf. Sci. **117**, 77 (1982).
[7]T. Toya, Y. Ohno, S. Ishi, and K. Nagai, *Proceedings of the 4th International Conference on Solid Surfaces and 3rd European Conference on Surface Sciences*, edited by D. A. Degras and M. Costa (Cannes, 1980), p. 141; personal communication (1983).
[8]W. L. Schaich, Phys. Lett. A **64**, 133 (1977).
[9]G. Doyen, *Proceedings of the 4th International Conference on Solid Surfaces and 3rd European Conference on Surface Sciences*, edited by D. A. Degras and M. Costa (Cannes 1980), p. 145; Vacuum **32**, 91 (1982).
[10]D. R. Horton, W. F. Banholzer, and R. I. Masel, Surf. Sci. **116**, 22 (1982).
[11]P. R. Norton, Surf. Sci. **44**, 624 (1974).
[12]T. Matsushima, Surf. Sci. **127**, 403 (1983).
[13]T. Matsushima, M. Hashimoto and I. Toyoshima, J. Catal. **58**, 303 (1979).
[14]T. Matsushima, J. Catal. **83**, 446 (1983).
[15]T. Matsushima, J. Phys. Chem. **88**, 98 (1984).
[16]R. L. Palmer and J. N. Smith, J. Chem. Phys. **60**, 1453 (1974).
[17]C. T. Campbell, G. Ertl, H. Kuipers, and J. Segner, J. Chem. Phys. **73**, 5862 (1980).
[18]T. Engel and G. Ertl, J. Chem. Phys. **69**, 1267 (1978).
[19]C. A. Becker, J. P. Cowin, L. Wharton, and D. J. Auerbach, J. Chem. Phys. **67**, 3394 (1977).
[20]G. B. Fisher and S. J. Schmieg, J. Vac. Sci. Technol. A **1**, 1064 (1983).
[21]T. Matsushima, J. Catal. **85**, 98 (1984).
[22]P. A. Thiel, J. T. Yates, Jr., and W. H. Weinberg, Surf. Sci. **82**, 22 (1979).
[23]J. Falconer and R. J. Madix, J. Catal. **48**, 262 (1977).
[24]P. A. Redhead, Vacuum **12**, 203 (1962).
[25]R. J. Koestner, M. A. Van Hove, and G. A. Somorjai, Surf. Sci. **107**, 439 (1981).
[26]P. A. Thiel, E. D. Williams, J. T. Yates, Jr., and W. H. Weinberg, Surf. Sci. **84**, 54 (1979).
[27]J. L. Gland and E. B. Kollin, J. Chem. Phys. **78**, 963 (1983).
[28]J. L. Gland, M. R. McClellan, and F. R. McFeely, J. Vac. Sci. Technol. A **1**, 1070 (1983).
[29]C. T. Campbell, S-K. Shi, and J. M. White, J. Vac. Sci. Technol. **16**, 605 (1979).
[30]C. T. Campbell, S-K. Shi, and J. M. White, J. Phys. Chem. **83**, 2255 (1979).
[31]C. T. Campbell, S-K. Shi, and J. M. White, Appl. Surf. Sci. **2**, 382 (1979).
[32]H. Conrad, G. Ertl, and J. Kuippers, Surf. Sci. **76**, 323 (1978).
[33]*Lange's Handbook of Chemistry 20th*, edited by J. A. Dean (McGraw–Hill, New York, 1979).
[34]T. Kobal, M. Senegacnik, and B. Barlic, J. Chem. Phys., **62**, 2740 (1975).
[35]N. K. Ray and A. B. Anderson, Surf. Sci. **119**, 35 (1982).
[36]D. A. Mantell, S. B. Ryali, B. L. Halpern, G. L. Haller, and J. B. Fenn, Chem. Phys. Lett. **81**, 185 (1981).
[37]S. L. Bernasek and S. R. Leone, Chem. Phys. Lett. **84**, 401 (1981).